

# Supporting Information

## Core-Shell Au@Metal-Oxide Nanoparticle Electrocatalysts for Enhanced Oxygen Evolution

*Alaina L. Strickler,<sup>†</sup> Maria Escudero-Escribano,<sup>†§</sup> and Thomas F. Jaramillo<sup>\*†‡</sup>*

<sup>†</sup>Department of Chemical Engineering, Stanford University, Stanford, California 94305, United States

<sup>§</sup> Nano-Science Center, Department of Chemistry, Universitetsparken 5, University of Copenhagen, DK-2100 Copenhagen, Denmark

<sup>‡</sup>SUNCAT Center for Interface Science and Catalysis, SLAC National Accelerator Laboratory, Menlo Park, California 94025, United States

\*Email: [jaramillo@stanford.edu](mailto:jaramillo@stanford.edu)

## Experimental Section:

### 1. Nanoparticle Synthesis

#### 1a. Au Nanoparticle Synthesis

Au nanoparticles were synthesized following a literature procedure.<sup>1</sup> Briefly, monodisperse 3 nm diameter particles were formed by combining 100 mg gold(III) chloride trihydrate (99.9+%, Fluka Chemie GMBH) with 10 mL 1,2,3,4-tetrahydronaphthalene (tetralin) (anhydrous 99%, Sigma-Aldrich) and 10 mL oleylamine (80-90%, Acros) in a round bottom flask. In a separate vial, 43.5 mg borane tert-butylamine complex (TBAB) (97%, Sigma-Aldrich) was combined with 1 mL oleylamine and 1 mL tetralin and sonicated until dissolved. This solution was then quickly injected into the round-bottom flask under vigorous stirring at room temperature in air to nucleate the gold nanoparticles. After reacting for one hour, the particles were collected by centrifuging with ethanol and stored in hexanes. Nanoparticle size can be easily adjusted by modifying reaction temperature and Au precursor concentration (see Figure S1).

#### 1b. Nickel Oxide Nanoparticle Synthesis

Nickel oxide nanoparticles were synthesized following a procedure previously developed.<sup>2</sup> Briefly, 0.5 mmol of nickel(II) acetylacetonate (95%, Sigma-Aldrich) was combined with 7.5 mL of oleylamine (70%, Aldrich) and 160  $\mu$ L of oleic acid (90%, Aldrich) in a round bottom flask. The solution was heated to 100°C in 20 minutes and held for an hour. After cooling to 90°C, a solution of 132 mg TBAB and 1 mL oleylamine was quickly injected under vigorous stirring to nucleate the nickel nanoparticles and reacted for 1 hr. Particles were separated by centrifugation with ethanol and stored in hexanes.

#### 1c. Au@NiO<sub>x</sub> Nanoparticle Synthesis

Gold-core nickel oxide-shell nanoparticles were synthesized by a method inspired by a synthesis for Ag@Ni.<sup>3</sup> First, 0.02 mmol of gold nanoparticles (in hexane solution) were combined with 0.1 mmol of nickel(II) acetylacetonate, 0.02 mmol of triphenylphosphine (99%, Sigma-Aldrich), 500  $\mu$ L oleylamine (70%, Aldrich), and 2 mL 1-octadecene (90%, Sigma-Aldrich) in a 25 mL three-neck round bottom flask. Under argon and vigorous stirring, the mixture was heated to 80°C for 20 minutes before being slowly heated (1-2°C/min) to 190°C and reacted for 40 minutes. Particles were separated by centrifugation with ethanol and isopropyl alcohol and stored in hexanes.

#### 1d. Cobalt Oxide Nanoparticle Synthesis

Cobalt nanoparticles were synthesized following a literature procedure.<sup>4</sup> Briefly, 70 mg of cobalt(II) nitrate hexahydrate (Sigma-Aldrich, reagent grade >98%) was combined with 300 mg octadecylamine (97%, Sigma-Aldrich), 100 mg triocylphosphine oxide (90%, Sigma-Aldrich) and 8 mL benzyl alcohol (99.8%, Sigma-Aldrich). After the mixture dissolved, it was gradually heated (3°C/min) to 140°C and held for ten minutes. The particles were isolated by centrifugation with isopropyl alcohol and redispersed in hexanes.

#### 1e. Au@CoO<sub>x</sub> Synthesis

Gold-core cobalt oxide-shell nanoparticles were synthesized following a method developed in a previous report.<sup>5</sup> First, 0.02 mmol of gold nanoparticles (in hexanes) were combined with 0.2 mmol of cobalt(II) acetylacetonate (97%, Sigma-Aldrich), 0.2 mmol of oleic acid, and 3 mL of oleylamine (70%). The mixture was heated under argon at 100°C for one hour. A mixture of 0.8 mmol TBAB in 400  $\mu$ L oleylamine was then injected and the solution was allowed to react for one hour. Particles were isolated via centrifugation with ethanol and stored in hexanes.

1f: CoFeO<sub>x</sub> (6 nm and 12 nm)

Cobalt/iron oxide nanoparticles were synthesized following a method developed previously.<sup>6</sup> 12 nm particles were synthesized by combining 0.25 mmol of cobalt(II) acetylacetonate, 0.25 mmol iron(III) acetylacetonate (97%, Sigma-Aldrich), 2.5 mmol 1,2-hexadecanediol (TCI America), 1.5 mmol oleylamine (80-90%), 1.5 mmol oleic acid, and 5 mL benzyl ether (98%, Sigma-Aldrich). The solution was heated to 200°C under argon for 30 minutes and then to reflux for 30 minutes. Nanoparticles were separated by centrifugation with ethanol and redispersed in hexanes. 6 nm particles were synthesized following the same procedure except heating rapidly to reflux in one heating step.

1g. Au@CoFeO<sub>x</sub>

Gold-core cobalt/iron oxide shell nanoparticles were synthesized following the same procedure described above for Au@CoO<sub>x</sub> nanoparticles. 0.02 mmol of gold nanoparticles were combined with 0.1 mmol of cobalt(II) acetylacetonate, 0.1 mmol iron(III) acetylacetonate, 0.2 mmol of oleic acid, and 3 mL of oleylamine (70%). The mixture was heated under argon at 100°C for one hour. 0.8 mmol TBAB in 400  $\mu$ L oleylamine was then injected and the solution was allowed to react for one hour. Nanoparticles were separated by centrifugation with ethanol and redispersed in hexanes.

1h. Fe Oxide Synthesis (3 nm and 14 nm)

Iron oxide nanoparticles were synthesized following a procedure developed previously.<sup>6</sup> 14 nm diameter particles were synthesized by combining 0.25 mmol iron(III) acetylacetonate, 1.25 mmol 1,2-hexadecanediol, 1.5 mmol oleylamine (80-90%), 1.5 mmol oleic acid, and 5 mL benzyl ether. The solution was heated to 200°C under argon for 30 minutes and then to reflux for 30 minutes. Nanoparticles were separated by centrifugation with ethanol and redispersed in hexanes. 3 nm diameter particles were synthesized following the same procedure but using phenyl ether as the solvent.

1g. Au/FeO<sub>x</sub> Synthesis

Gold-iron oxide peanut nanoparticles were synthesized in a similar method to the iron only nanoparticles. First, 0.02 mmol of gold nanoparticles were combined with 0.1 mmol of iron(III) acetylacetonate, 0.625 mmol 1,2-hexadecanediol, 0.75 mmol oleic acid, 0.75 mmol oleylamine (80-90%), and 2.5 mL benzyl ether. The solution was heating in a 25 mL three-neck round bottom flask at 4°C/min to 200°C for 30 minutes under vigorous stirring. The solution was then heated to reflux at 3°C/min and reacted for 30 minutes. Particles were precipitated with ethanol and centrifugation and stored in hexanes.

Au<sub>3nm</sub>/FeOx<sub>9nm</sub> peanut particles were synthesized following a literature method.<sup>7</sup> 0.0355 mmol of 3 nm Au nanoparticles, 1.214 mmol of OAm, 1.214 mmol of OA, and 20 mL of 1-octadecene were combined in a vigorously stirred round bottom flask. The solution was heated to 80°C under vacuum for 30 min. Under Ar atmosphere, 0.1 mL of iron pentacarbonyl (Sigma-Aldrich, >99.99%) was then injected and the temperature was increased to 180°C for 30 min. The temperature was increased further to 250°C for 30 min then cooled to 100°C for 10 min in air.

## 2. Electrode Preparation

### 2a. Catalyst Ink Preparation

Nanoparticles were supported by combining an appropriate amount of nanoparticle hexane solution with 10 mg/mL carbon black (Vulcan XC-72) hexane solution to achieve a 20 wt% nanoparticle metal loading. The resulting mixture was sonicated for one hour then stirred at room temperature uncapped to evaporate the hexane solvent. The dry ink was then dispersed in 1 mL isopropyl alcohol and 15  $\mu$ L ion exchanged Nafion 117 solution (~5% in a mixture of lower aliphatic alcohols and water, Aldrich). Ion exchanged Nafion was made by combining 1 mL Nafion 117 with 500  $\mu$ L 0.1 M potassium hydroxide and stirring for two days. Inks were sonicated for 30 minutes prior to electrochemical testing. The quantity of nanoparticles used was chosen so that 20  $\mu$ L of catalyst ink yielded 1  $\mu$ mol of 3d transition metal per cm<sup>2</sup> on a 0.196 cm<sup>2</sup> polished glassy carbon disk.

### 2b. Fe-Free Catalyst Electrode Preparation

To remove iron impurities from the carbon black support, 1 g of Vulcan XC-72 was stirred in 10 mL of 2 M hydrochloric acid at 50°C overnight. The Fe-free carbon black was then filtered and washed with deionized water until a neutral pH was achieved. The powder was then dried at 100°C in a box furnace. Fe-free catalyst inks were then prepared as described above. Glassy carbon disks were cleaned to remove iron impurities by soaking in dilute nitric acid (10 vol%) overnight.

### 2c. Electrochemical Set-up

Fe containing nanoparticles were tested in a three-electrode rotating disk electrode (RDE) set-up with an catalyst ink coated polished glassy carbon disk working electrode (0.196 cm<sup>2</sup>), a saturated Ag/AgCl reference electrode (1.01 V vs. RHE), a Pt wire counter electrode, and 1 M potassium hydroxide (KOH) electrolyte. Nanoparticle catalysts were deposited by dropping 10  $\mu$ L of catalyst ink onto the glassy carbon disk attached to an inverted RDE and rotating at 700 rpm until dry. This process was repeated for a total of 20  $\mu$ L to achieve a 3d transition metal loading of 1  $\mu$ mol/cm<sup>2</sup>. This loading was determined by the amount of metal used during synthesis and is therefore a conservative estimate as yield is likely well below 100%.

### 2d. Fe-free Electrochemical Set-up

For Fe-free experiments, 1 M KOH electrolyte solution was purified following a procedure developed by the Boettcher group.<sup>8</sup> A Teflon beaker was used as the electrochemical cell. A Teflon 1 M KOH Hg/HgO reference electrode (927 mV vs. RHE) (CHI152, CH Instruments) and a Pt

wire counter electrode were used. A glass gas dispersion tube was cleaned with 1 M sulfuric acid and submerged ~5 mm to purge the electrolyte with oxygen during OER experiments. The Teflon disk holder and electrochemical cell were cleaned overnight with piranha solution prior to use. Non-iron containing catalysts were deposited on cleaned GCDs attached to an inverted RDE as described above.

## 2e. Electrochemical Testing

Electrochemical experiments were performed at 1600 rpm in oxygen saturated electrolyte. OER cyclic voltammograms (CVs) were collected at 10 mV/s from 1 V vs. RHE until the geometric current density reached ~ 15 mA/cm<sup>2</sup>. All current densities in this work are reported on a geometric basis. The solution series resistance was compensated at 85% using impedance spectroscopy with the PEIS measured at open circuit. Accelerated cycling of the nickel catalysts was performed between 0.25 and 1.6 V vs. RHE at 200 mV/s as this was found to accelerate the activation of nickel sites, particularly for Au@NiO<sub>x</sub> catalysts. Chronopotentiometric stability tests were performed at 1600 rpm in 1 M KOH by recording the overpotential required to maintain a current density of 10 mA/cm<sup>2</sup><sub>geo</sub> for 2 hours.

## 3. Materials characterization

### 3a. TEM

Nanoparticle samples were prepared for transmission electron microscopy (TEM) imaging by dropcasting the solution onto ultrathin carbon on holey carbon support 400-mesh copper TEM grids (Ted Pella). A FEI Tecnai operated at 200 kV was used to obtain micrographs. Average particle size and dispersion were analyzed with ImageJ software. Energy dispersive spectroscopy (EDS) spectra were obtained in TEM and scanning TEM (STEM) modes using an EDAX SUTW (super ultra thin window) and analyzer with 0.3 srads EDS solid angle. Line profiles were collected in STEM mode using a 12 second collection time and drift correction between points. EDS profile fits and peak integrations were performed using Tecnai Imaging Analysis (TIA) software.

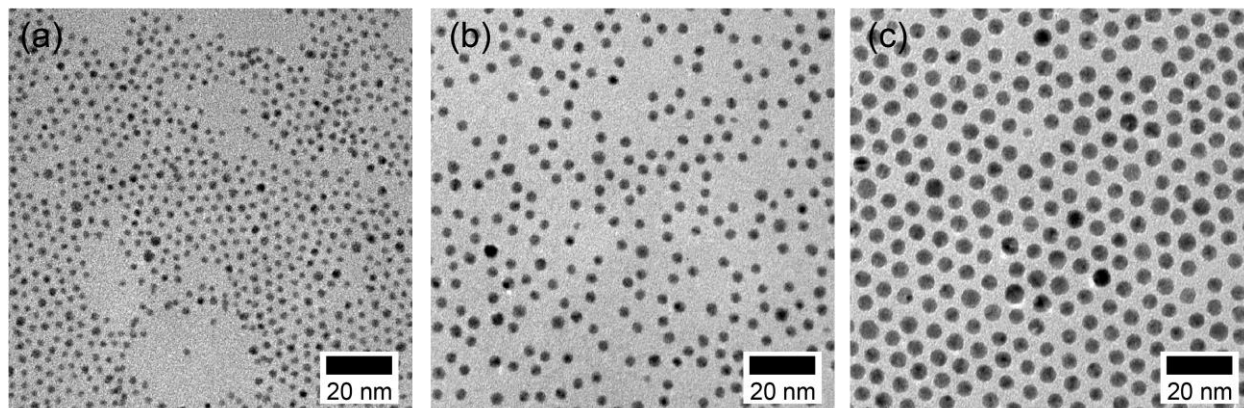


**Figure S1.** (a)  $1.9 \pm 0.3$  nm, (b)  $3.3 \pm 0.4$  nm, and (c)  $5.0 \pm 0.4$  nm diameter Au nanoparticles synthesized using the above described method at  $45^{\circ}\text{C}$ ,  $25^{\circ}\text{C}$ , and at  $20^{\circ}\text{C}$  with double the gold precursor concentration, respectively.

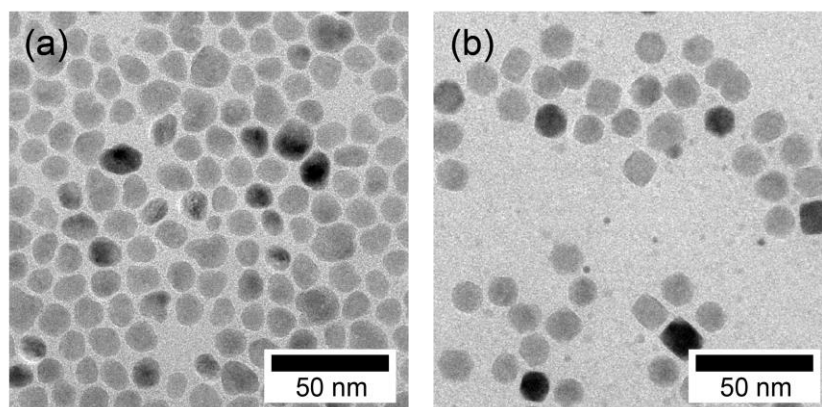


**Figure S2.** TEM micrographs of (a) CoFeO<sub>x</sub> nanoparticles ( $11.7 \pm 3.4$  nm) and (b) FeO<sub>x</sub> nanoparticles ( $13.7 \pm 1.3$  nm).

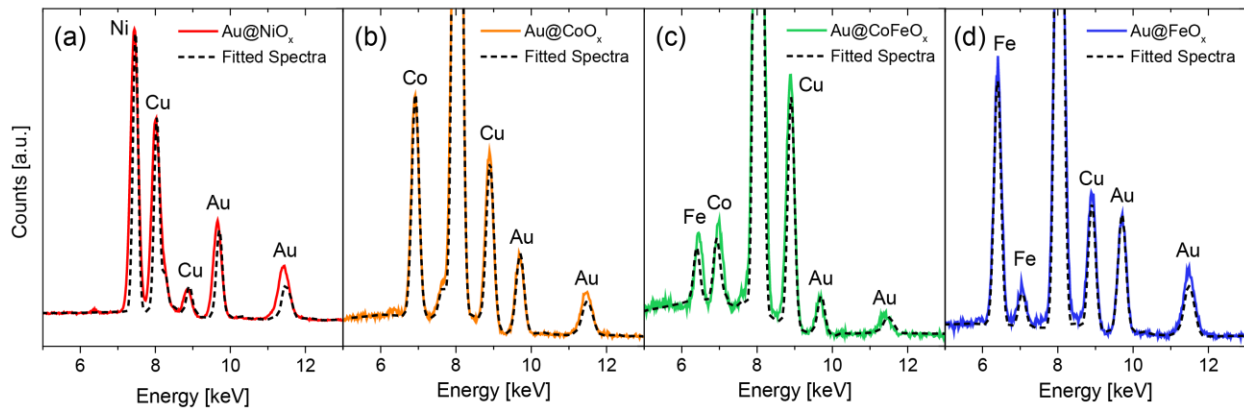


**Figure S3.** TEM-EDS spectra for (a) Au@NiO<sub>x</sub>, (b) Au@CoO<sub>x</sub>, (c) Au@CoFeO<sub>x</sub>, and (d) Au/FeO<sub>x</sub> nanoparticles. Ni, Co, Fe, and Cu K peaks and Au L peaks were fitted using TIA software. The Cu signal is from the Cu TEM grid. Due to the similarity in k-factors between Co and Fe, their integrated peak ratio can be used to approximate their relative composition without the use of standards. Using Tia software to fit K transition peaks, it was found that Au@CoFeO<sub>x</sub> has a molar ratio of 1:1 Co:Fe as expected from synthesis composition.

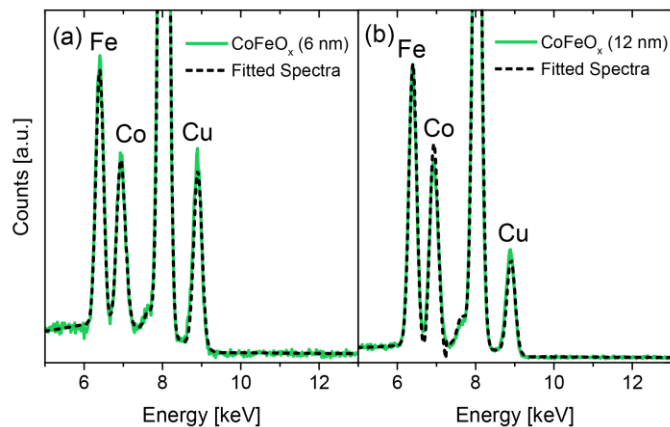


**Figure S4.** TEM-EDS spectra for (a) 6 nm CoFeO<sub>x</sub> and (b) 12 nm CoFeO<sub>x</sub> nanoparticles. Integrated Co and Fe K peaks indicate the nanoparticles are slightly Fe rich with an approximate molar ratio of 60:40 Fe:Co.

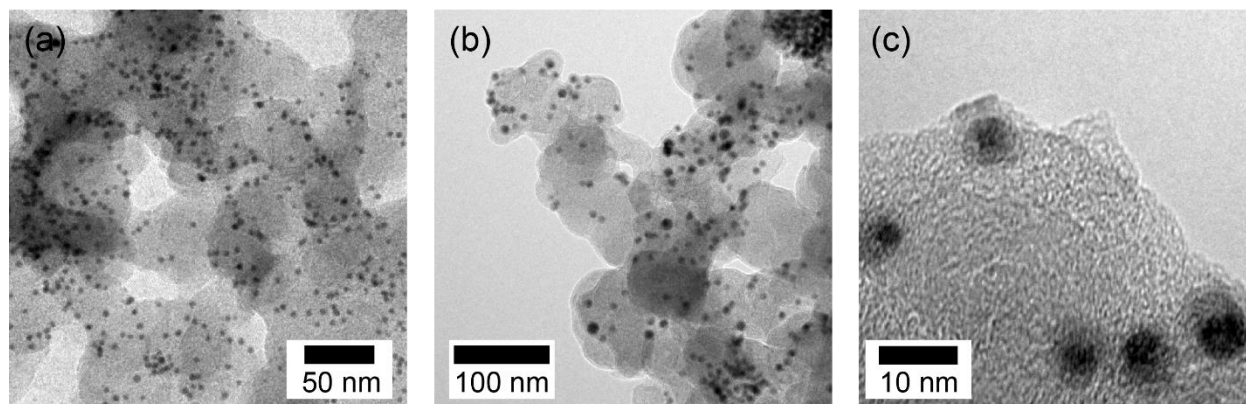


**Figure S5.** TEM micrographs of (a) Au@CoFeO<sub>x</sub> /C and (b-c) Au@NiO<sub>x</sub>/C supported nanoparticles.

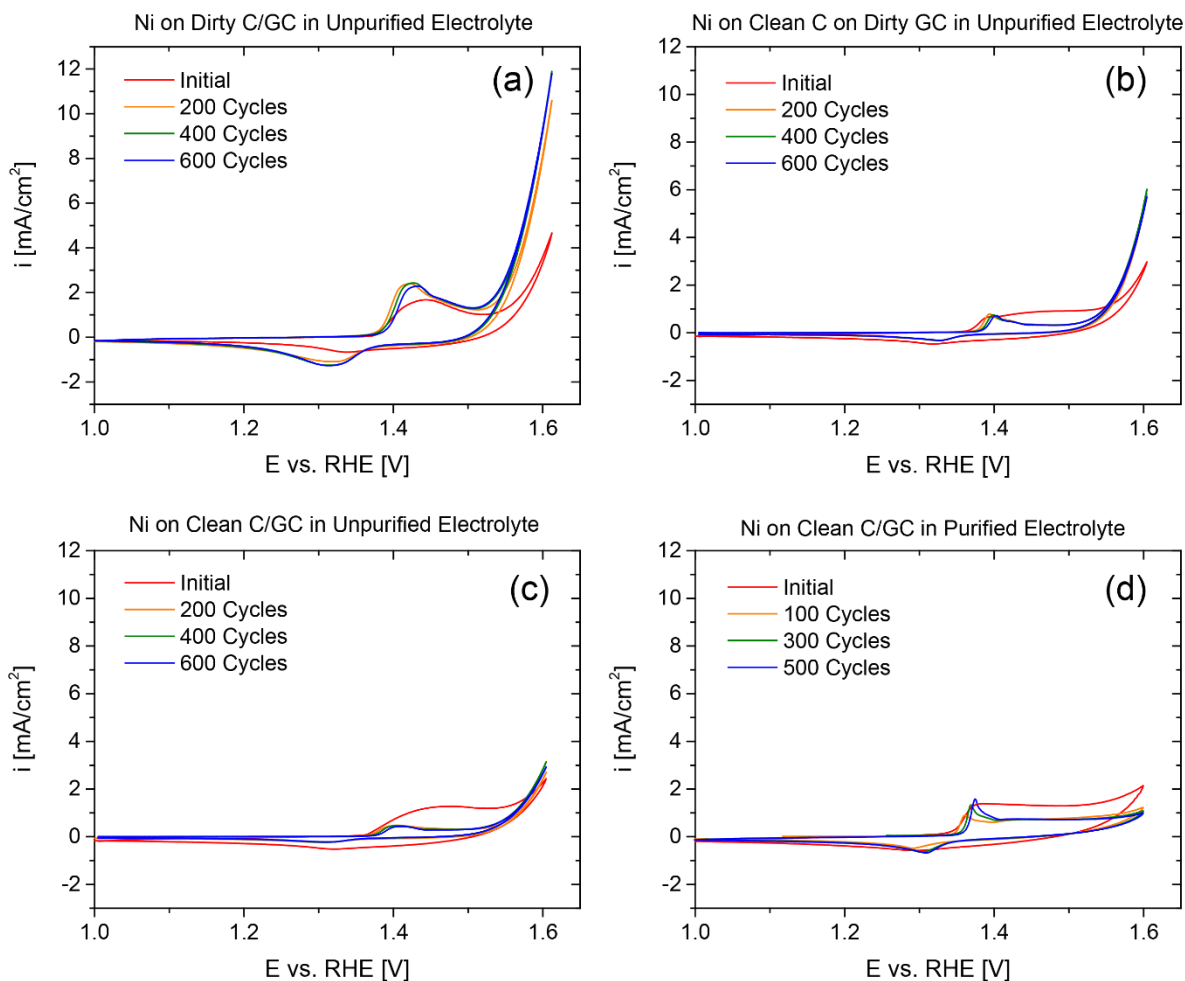


**Figure S6.** The effect of iron purification on the OER activity of  $\text{NiO}_x/\text{C}$  nanoparticles. Electrochemical testing was performed in 1 M KOH at 1600 rpm and 10 mV/s in oxygen saturated electrolyte with a catalyst loading of  $20 \mu\text{g}_{\text{Ni}}/\text{cm}^2$ . Accelerated cycling was performed between 0.25 and 1.6 V vs. RHE for the specified number of cycles to enhance the evolution of activity. (a)  $\text{NiO}_x$  nanoparticles on uncleaned carbon black and an uncleaned glassy carbon disk (GCD) in unpurified electrolyte. (b)  $\text{NiO}_x$  nanoparticles on cleaned carbon black and an uncleaned GCD in unpurified electrolyte. (c)  $\text{NiO}_x$  nanoparticles on cleaned carbon black and a cleaned GCD in unpurified electrolyte. (d)  $\text{NiO}_x$  nanoparticles on cleaned carbon black and a cleaned GCD in purified electrolyte. It can be seen that the cleaning of all three components (carbon black, the GCD, and the electrolyte) is required to eliminate iron contamination.

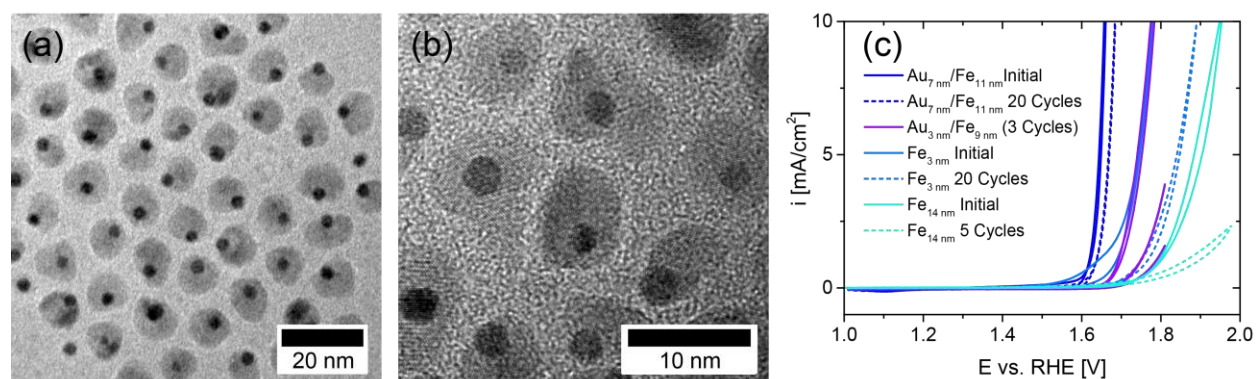


**Figure S7.** (a, b) TEM micrographs of Au/FeO<sub>x</sub> nanoparticles synthesized by injection of Fe(CO)<sub>5</sub>. Particles have a peanut morphology with  $2.9 \pm 0.5$  nm Au particles attached to  $9.4 \pm 0.7$  nm FeO<sub>x</sub> particles. (c) Cyclic voltammograms of Au/FeO<sub>x</sub> and FeO<sub>x</sub> particles in O<sub>2</sub> saturated 1 M KOH at 10 mV/s and 1600 rpm. The Au<sub>3</sub> nm/Fe<sub>9</sub> nm nanoparticles pictured here display decreased OER activity and stability compared to the Au<sub>7</sub> nm/Fe<sub>11</sub> nm shown here and in the main text and have similar initial activity to the 3 nm FeO<sub>x</sub> nanoparticles. This is likely a result of the decreased FeO<sub>x</sub>/Au interfacial area compared to the Au<sub>7</sub> nm/Fe<sub>11</sub> nm particles impairing the ability of electrons to reach the conductive support. The smaller 3 nm FeO<sub>x</sub> particles are less conductivity limited and have a similar initial activity to the larger FeO<sub>x</sub> nanoparticles with a small Au interfacial area, Au<sub>3</sub> nm/Fe<sub>9</sub> nm. This illustrates that for FeO<sub>x</sub>, the presence of Au as well as the amount of surface in contact with the Au are important parameters for achieving high activity.

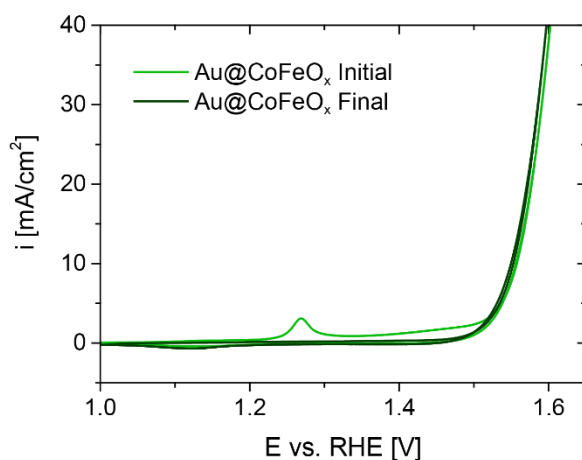


**Figure S8.** Cyclic voltammograms of Au@CoFeO<sub>x</sub> at 10 mV/s and 1600 rpm in oxygen saturated 1 M KOH before and after a 2 hour chronopotentiometric stability test at 10 mA/cm<sup>2</sup>. No decay in catalytic activity is observed after the stability test.

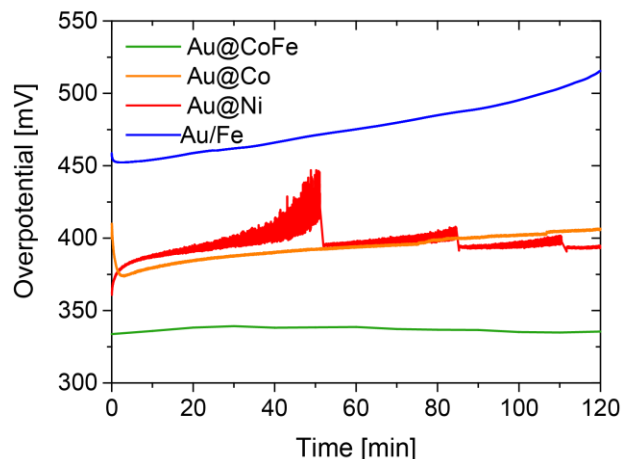


**Figure S9.** Chronopotentiometry at  $10 \text{ mA/cm}^2$  for 2 hr in  $\text{O}_2$  saturated 1 M KOH (purified for Fe-free catalysts) at 1600 rpm. Excessive bubble formation on the  $\text{Au@NiO}_x$  catalyst surface resulted in noise in the data.

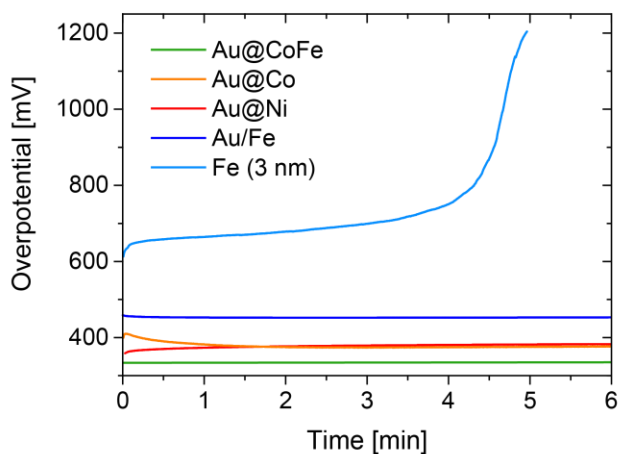


**Figure S10.** Chronopotentiometry at  $10 \text{ mA/cm}^2$  in 1 M KOH at 1600 rpm of core-shell catalysts compared to 3 nm diameter  $\text{FeO}_x$  nanoparticles illustrating the instability of 3 nm  $\text{FeO}_x$  after ~4 minutes. This instability is likely due to  $\text{FeO}_x$  dissolution to  $\text{FeO}_4^{2-}(\text{aq})$  at high pH and potential. The high overpotential required to reach  $10 \text{ mA/cm}^2$  for 3 nm  $\text{FeO}_x$  both increases the rate of Fe dissolution relative to  $\text{Au/FeO}_x$  as well as decreases the stability of the carbon black support leading to the complete delamination of the catalyst ink after ~4 min when the activity approaches that of bare glassy carbon. The lower overpotential of  $\text{Au/FeO}_x$  retards Fe dissolution and increases carbon stability; however, an even further decrease in overpotential is necessary to maintain long-term stability of this catalyst as it gradually decays and partially delaminates over the 2 hours of testing.

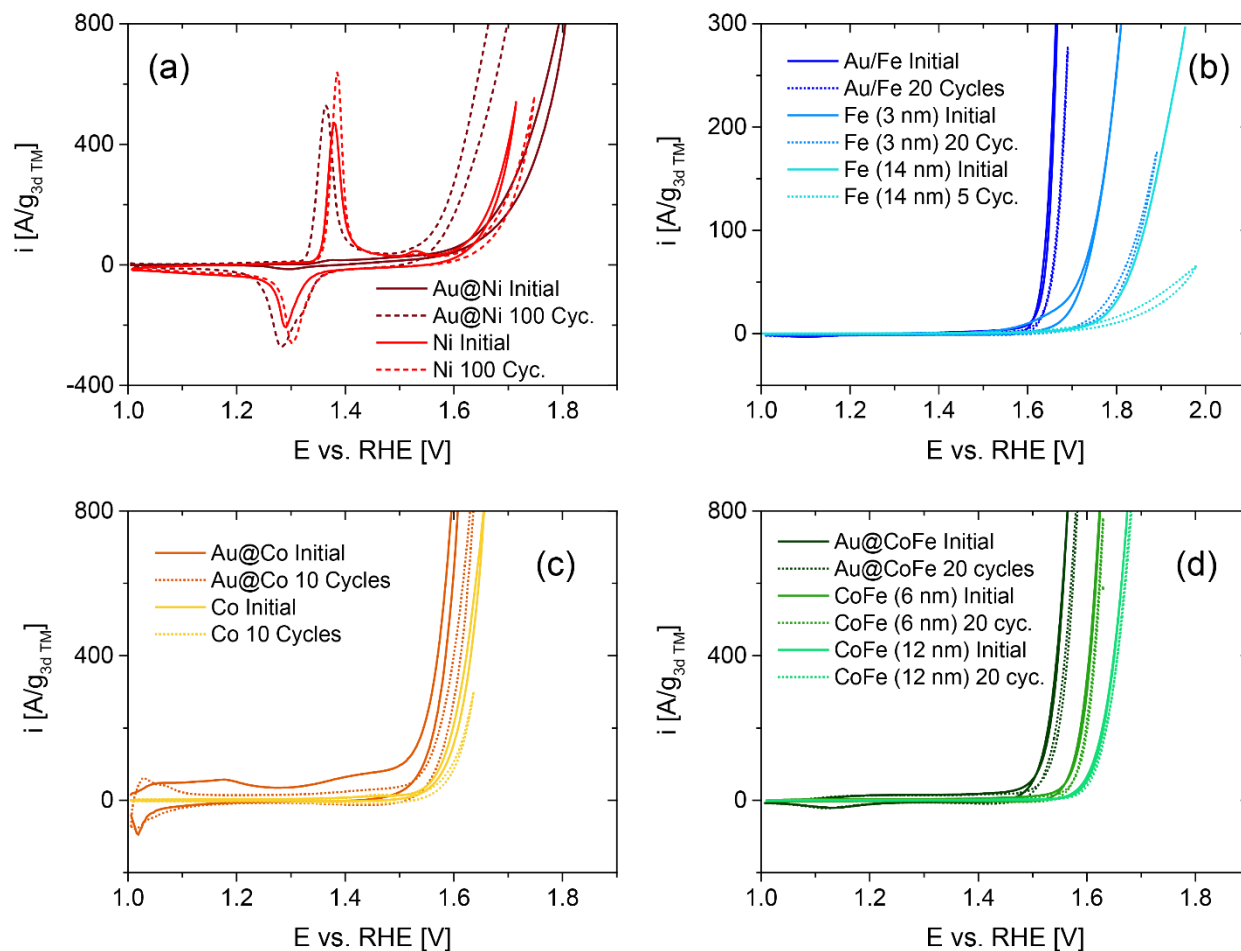


**Figure S11.** Electrochemical cyclic voltammograms of nanoparticle catalysts in O<sub>2</sub> saturated 1 M KOH (purified for Fe-free catalysts) at 10 mV s<sup>-1</sup> and 1600 rpm with solution resistance compensation normalized by ICP-MS determined 3d-transition metal mass. (a) Au@NiO<sub>x</sub> compared to NiO<sub>x</sub> nanoparticles initially and after 100 activation cycles from 0.25 to 1.6 V vs. RHE at 200 mV s<sup>-1</sup>. (b) Au/FeO<sub>x</sub> compared to 3 nm and 14 nm FeO<sub>x</sub> particles initially and after repeated cycling. (c) Au@CoO<sub>x</sub> and CoO<sub>x</sub> nanoparticles initially and after 10 cycles. (d) Au@CoFeO<sub>x</sub> compared to 6 nm and 12 nm CoFeO<sub>x</sub> nanoparticles initially and after 20 cycles. Au containing nanoparticles demonstrate enhanced OER activity compared to their corresponding pure 3d metal-oxide counterparts on a mass activity basis.

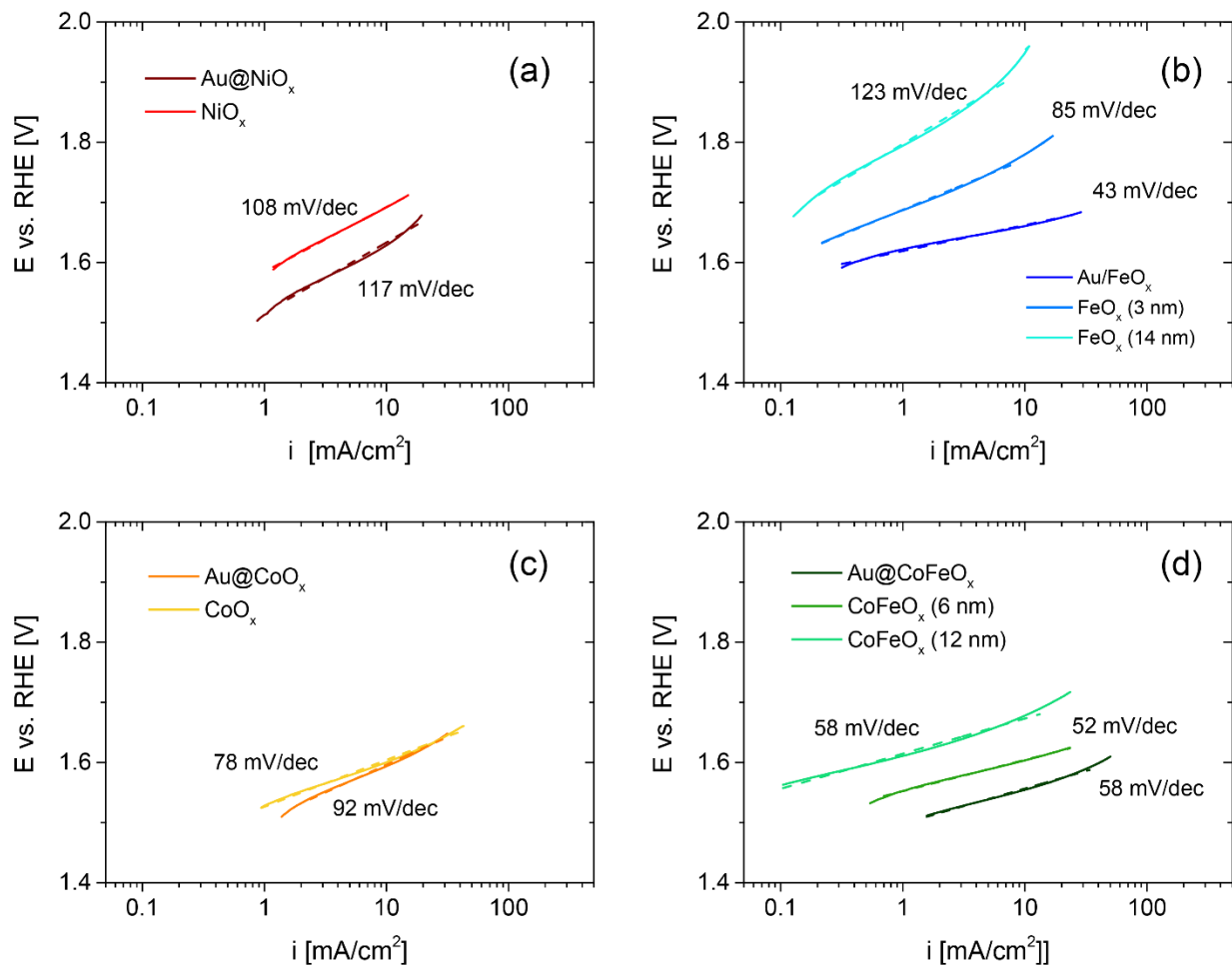


**Figure S12.** Tafel plots of nanoparticle catalysts in O<sub>2</sub> saturated 1 M KOH (purified for Fe-free catalysts) at 10 mV s<sup>-1</sup> and 1600 rpm with solution resistance compensation. (a) Au@NiO<sub>x</sub> compared to NiO<sub>x</sub> nanoparticles initially and after 100 activation cycles from 0.25 to 1.6 V vs. RHE at 200 mV s<sup>-1</sup>. (b) Au/FeO<sub>x</sub> compared to 3 nm and 14 nm FeO<sub>x</sub> particles initially and after repeated cycling. (c) Au@CoO<sub>x</sub> and CoO<sub>x</sub> nanoparticles initially and after 10 cycles. (d) Au@CoFeO<sub>x</sub> compared to 6 nm and 12 nm CoFeO<sub>x</sub> nanoparticles initially and after 20 cycles. Tafel slopes are consistent with those found previously for electrodeposited films.<sup>9</sup> For Ni, Co, and CoFe systems, Au appears to have a significant effect on the OER onset potential but little effect on the Tafel slope indicating that for these materials, Au does not change the rate limiting step of the reaction but instead reduces the limiting potential. For Fe systems, Au significantly decreases the Tafel slope relative to FeO<sub>x</sub>-only nanoparticles. The comparatively high Tafel slope of FeO<sub>x</sub> is likely due to poor conductivity and stability of the FeO<sub>x</sub> nanoparticles.

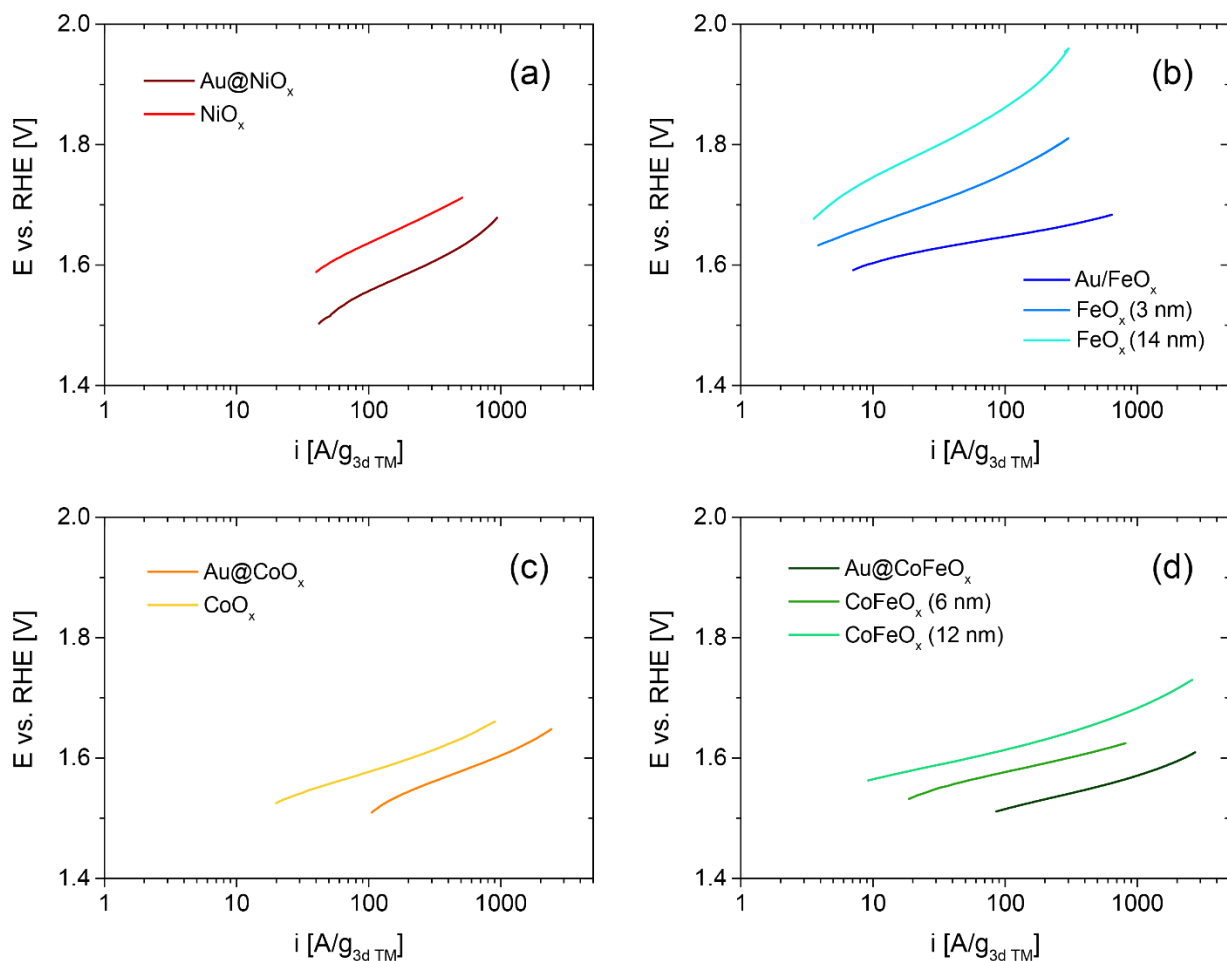


**Figure S13.** Potential versus mass activity for nanoparticle catalysts in  $\text{O}_2$  saturated 1 M KOH (purified for Fe-free catalysts) at  $10 \text{ mV s}^{-1}$  and 1600 rpm with solution resistance compensation. (a)  $\text{Au@NiO}_x$  compared to  $\text{NiO}_x$  nanoparticles initially and after 100 activation cycles from 0.25 to 1.6 V vs. RHE at  $200 \text{ mV s}^{-1}$ . (b)  $\text{Au/FeO}_x$  compared to 3 nm and 14 nm  $\text{FeO}_x$  particles initially and after repeated cycling. (c)  $\text{Au@CoO}_x$  and  $\text{CoO}_x$  nanoparticles initially and after 10 cycles. (d)  $\text{Au@CoFeO}_x$  compared to 6 nm and 12 nm  $\text{CoFeO}_x$  nanoparticles initially and after 20 cycles.

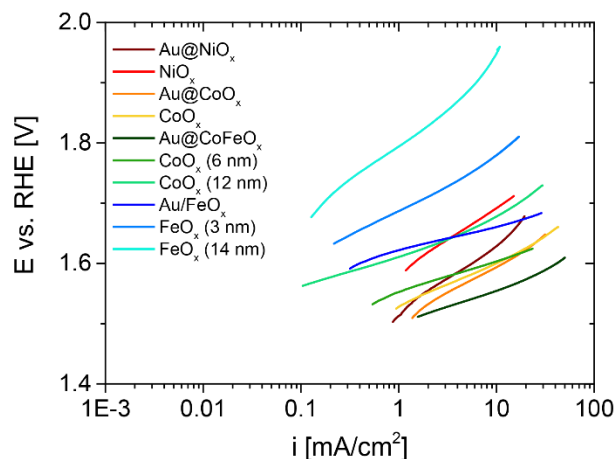


**Figure S14.** Tafel Plot of nanoparticle catalysts in O<sub>2</sub> saturated 1 M KOH (purified for Fe-free catalysts) at 10 mV s<sup>-1</sup> and 1600 rpm with solution resistance compensation.

**Table S1.** Activity Summary

Catalyst	Diameter [nm]	$\eta_{10 \text{ mA/cm}^2}$	$\eta_{300 \text{ A/g}}$	$i_{\eta=350 \text{ mV}}$ [A/g <sub>3d TM</sub> ]	Tafel Slope [mV/dec]
NiO <sub>x</sub>	3.4 ± 1.2	481 ± 11	429 ± 22	35	108
Au@NiO <sub>x</sub>	8.3 ± 2.0	394 ± 18	386 ± 12	170	117
CoO <sub>x</sub>	8.3 ± 1.7	380 ± 7	381 ± 6	110	78
Au@CoO <sub>x</sub>	6.3 ± 0.4	367 ± 6	332 ± 4	530	92
CoFeO <sub>x</sub> (6 nm)	6.1 ± 1.7	367 ± 2	370 ± 2	120	52
CoFeO <sub>x</sub> (12 nm)	11.7 ± 3.4	441 ± 13	412 ± 4	20	58
Au@CoFeO <sub>x</sub>	7.1 ± 0.4	328 ± 3	312 ± 2	1350	58
FeO <sub>x</sub> (3 nm)	3.0 ± 0.6	557 ± 12	610 ± 30	30*	85
FeO <sub>x</sub> (14 nm)	13.7 ± 1.3	714 ± 17	735 ± 6	5*	123
Au/FeO <sub>x</sub>	11 ± 3	439 ± 6	446 ± 8	580*	43

\*Mass activity taken at 450 mV overpotential.

## References

- (1) Peng, S.; Lee, Y.; Wang, C.; Yin, H.; Dai, S.; Sun, S. *Nano Res.* **2008**, *1* (3), 229–234.
- (2) Metin, O.; Mazumder, V.; Özkaz, S.; Sun, S. *J. Am. Chem. Soc.* **2010**, *132* (5), 1468–1469.
- (3) Guo, H.; Chen, Y.; Chen, X.; Wen, R.; Yue, G.-H.; Peng, D.-L. *Nanotechnology* **2011**, *22* (19), 195604.

- (4) Chou, N. H.; Ross, P. N.; Bell, A. T.; Tilley, T. D. *ChemSusChem* **2011**, *4* (11), 1566–1569.
- (5) Zhuang, Z.; Sheng, W.; Yan, Y. *Adv. Mater.* **2014**, *26* (23), 3950–3955.
- (6) Sun, S.; Zeng, H.; Robinson, D. B.; Raoux, S.; Rice, P. M.; Wang, S. X.; Li, G. *J. Am. Chem. Soc.* **2004**, *126* (1), 273–279.
- (7) Shevchenko, E. V.; Bodnarchuk, M. I.; Kovalenko, M. V.; Talapin, D. V.; Smith, R. K.; Aloni, S.; Heiss, W.; Alivisatos, A. P. *Adv. Mater.* **2008**, *20* (22), 4323–4329.
- (8) Trotochaud, L.; Young, S. L.; Ranney, J. K.; Boettcher, S. W. *J. Am. Chem. Soc.* **2014**, *136* (18), 6744–6753.
- (9) Burke, M. S.; Zou, S.; Enman, L. J.; Kellon, J. E.; Gabor, C. A.; Pledger, E.; Boettcher, S. W. *J. Phys. Chem. Lett.* **2015**, *6* (18), 3737–3742.